$Y\bar{Y}$ PRODUCTION BY 5.7 GeV/c ANTIPROTONS IN HYDROGEN

R. Bock, A. Cooper, B. R. French, R. LeviSetti *

CERN, Switzerland

D. Revel, B. Tallini, S. Zylberajch

C. E. N., Saclay, France

(Presented by B. R. FREHCH)

INTRODUCTION

The 81 cm Saclay hydrogen bubble chamber was exposed to 4×10^6 antiprotons of 5.7 GeV/c.

Table

Reaction	σ, μb
$p\bar{p} \to \Lambda^0\bar{\Lambda}^0$	40±10
$\Lambda^0\bar{\Sigma}^0$+c. c.	30±8
$\Sigma^+\bar{\Sigma}^+$	37±10
$\Sigma^-\bar{\Sigma}^-$	2±6
$\Sigma^+\Lambda^0\pi^-$+c. c.	45±8 → ~12 $\Sigma^+\bar{Y}_1^{*+}$(1385)+cc; → ~6 $\Lambda\bar{Y}_0^*$ (1405)+cc
$\Sigma^-\bar{\Lambda}^0\pi^+$+c. c.	20±5 → ~1 $\Sigma^-\bar{Y}^{*-}$ (1385)+cc; → ~5 ΛY_0^* (1405)+cc
$\Sigma^+\bar{\Sigma}^0\pi^-$+c. c.	25±7
$\Sigma^-\bar{\Sigma}^0\pi^+$+c. c.	10±4
$\Lambda^0\bar{\Lambda}^0\pi^0$	78±13 → ~50 $\Lambda\bar{Y}_1^*$ (1385)+cc; → ~16 $\Lambda\bar{Y}^*$ (1660)+cc
$\Lambda^0K^0\bar{n}$+c. c.	60±16 → ~7 $\Lambda\bar{Y}_0^*$ (1520)+cc
$\Lambda^0K^+\bar{p}$+c. c.	29±6 → ~6 $\Lambda\bar{Y}_0^*$ (1520)+cc
$\Sigma^0K^+\bar{p}$+c. c.	13±5
$\Sigma^+K^0\bar{p}$+c. c.	20±8
$\Sigma^+\bar{\Lambda}^0\pi^-\pi^0$+c. c.	41±8
$\Sigma^-\bar{\Lambda}^0\pi^+\pi^-$+c. c.	19±5
$\Sigma^0\bar{\Lambda}^0\pi^+\pi^-$+c. c.	16±4
$\Lambda^0\bar{\Lambda}^0\pi^+\pi^-$	27±5
$\Sigma^+\pi^-K^0\bar{n}$+c. c.	40±10
$\Sigma^+\bar{p}K^0\pi^0$+c. c.	24±8
$\Lambda^0\bar{\Lambda}^0\pi^+\pi^-\pi^0$	43±9

* Guggenheim Fellow, on leave of absence from the University of Chicago.

The spread in the beam momentum was estimated at ± 1%.

The contamination of the beam, obtained from δ-ray counting, was 6% μ's and 2% π's.

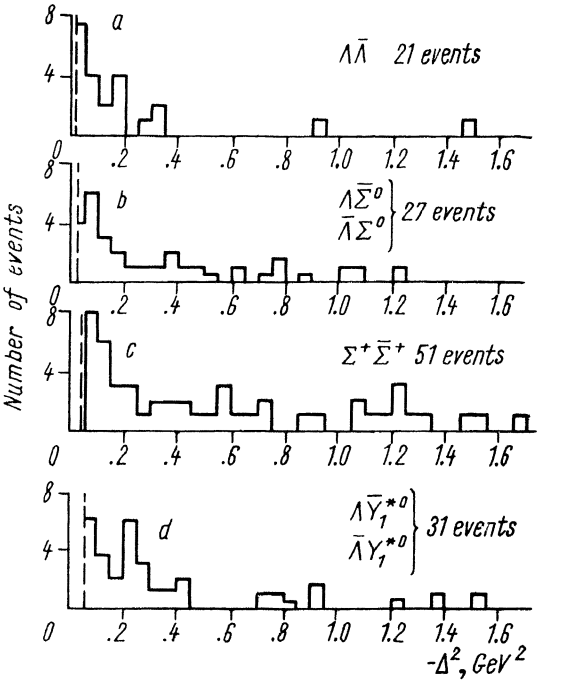

Fig. 1. $-\Delta^2$ distributions for $p\bar{p}$ reactions leading to two-body final states.

A value of 0.0625 gm/cm³ has been used for the density of liquid hydrogen in the computation of cross sections.

Presented here are the preliminary results, derived from half the available data, concerning hyperon-antihyperon production in two, three, four and five-body final states. Results on similar works at 3, 3.6 and 4 GeV/c antiproton momenta have been reported elsewhere [1].

The cross sections for the various reaction channels studied here are summarised in Table.

I. $Y\bar{Y}$ FINAL STATES

The Δ^2 distribution for the two-body reactions $\Lambda\bar{\Lambda}$, $\Lambda\bar{\Sigma}^0$, and $\Sigma^+\bar{\Sigma}^+$ are shown in Fig. 1. A common feature is the peaking of the distributions at low Δ^2 values, corresponding

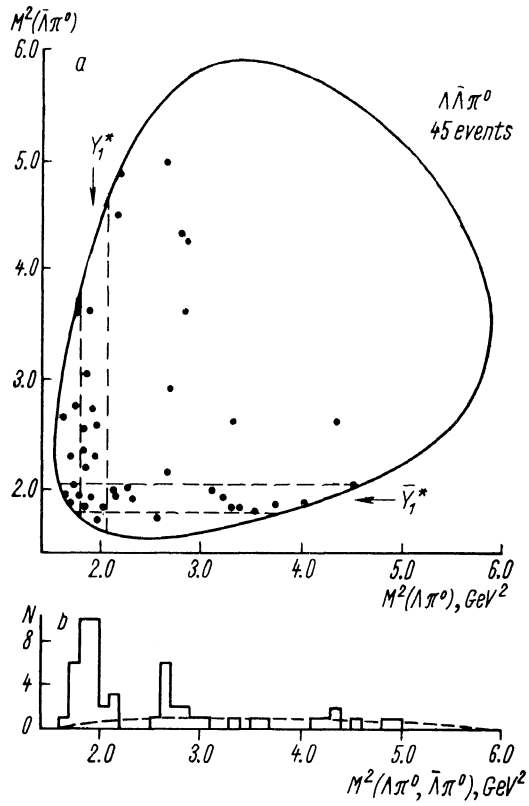

Fig. 2. Dallitz plot for $p\bar{p} \to \Lambda\bar{\Lambda}\pi^0$ events. The phase space mass distribution, outside of the $Y_1^*(1385)$ bands, is indicated by the dashed line in (b).

to the strong forward (backward) collimation of the antihyperons (hyperons) in the c. m. s.

While for $\Lambda\bar{\Lambda}$ the fraction of events having $\Delta^2 > 0.25$ is $\sim$0.25, for the $\Lambda\bar{\Sigma}^0$ and the $\Sigma^+\bar{\Sigma}^+$ this fraction becomes 0.5 and 0.6, respectively.

Thus the general character of the production mechanism is similiar to that observed in the region of 3 to 4 GeV/c. However, we note that in the present set of data there is no evidence for $\Sigma^-\bar{\Sigma}^-$ production.

The high $\Sigma^+\bar{\Sigma}^+$ cross section relative to that for $\Sigma^-\bar{\Sigma}^-$ production on one side, and the strong forward (backward) collimation of the antibaryons (baryons) on the other, are suggestive of an exchange production mechanism, where the contribution of the exchange of a charge $Q = 2$, strangeness $S = 1$ system is small compared with that of $Q = 0,1$ systems.

II. $\bar{Y}Y\pi$ AND $\bar{Y}KN$ FINAL STATES

1) $\Lambda^0\bar{\Lambda}^0\pi$ events: The Dalitz plot of Fig. 2 shows that these events proceed mainly via the quasi-two-body reaction $p\bar{p} \to \Lambda Y^{*+}$ c. c. with $\sim$65% $Y_1^*(1385)$ and $\sim$22% $Y^*(1660)$. The Δ^2 distribution, for the $Y_1^*(1385)$ producing reactions, of Fig. 1, d is similar to those for the two-body $Y\bar{Y}$ events.

2. $\Sigma^+\bar{\Lambda}\pi^- +$ c. c. and $\Sigma^-\bar{\Lambda}\pi^+ +$ c. c. Evidence for the production of $Y_1^*(1385)$ and some $Y_1^*(1405)$ and $Y_1^*(1520)$ resonances in these reactions is exhibited in the Dalitz plot shown in Fig. 3.

Several of the features of these reactions can be understood in terms of the exchange mechanism mentioned above, viz.,

a) once again the antihyperons show a strong forward peaking in c. m. s.;

b) in the reaction $\Sigma^-\pi^+\bar{\Lambda} +$ c. c. the $\bar{Y}_1^{*-} \to \bar{\Lambda} + \pi^+$, corresponding to the $Q = 2$ exchange in the above model, is absent;

c) after subtraction of the $Y_1^*(1385)$, $Y_0^*(1405)$ and $Y_0^*(1520)$ contributions the ratio $\sigma(\Sigma^+\pi^-\bar{\Lambda})/\sigma(\Sigma^-\pi^+\bar{\Lambda})$ equals about 3;

d) in those reactions where a Σ^0 replaces the $\bar{\Lambda}^0$ we find $\sigma(\Sigma^+\pi^-\bar{\Sigma}^0)/\sigma(\Sigma^-\pi^+\bar{\Sigma}^0)$ about 2.5;

e) for the four-body reactions, where an extra π^0 is produced, the ratio $\sigma(\Sigma^+\pi^-\bar{\Lambda}^0\pi^0)/\sigma(\Sigma^-\pi^+\bar{\Lambda}^0\pi^0)$ also equals about 2.5.

3. $\Lambda K^+p^- +$ c. c. and $\Lambda K^0\bar{n} +$ c. c. The only significant departure from a uniform population of the Dalitz plots in these reactions is observed in the region of the $Y_0^*(1520)$ as can be seen in Fig. 4.

III. $Y\bar{Y}\pi\pi$ FINAL STATES

$\Lambda\bar{\Lambda}\pi^+\pi^-$: This channel is dominated by the production of Y_1^*, $(\bar{Y}_1^*)$ via a peripheral-type mechanism. Thus the $M(\Lambda\pi, \bar{\Lambda}\pi)$ vs. $\cos\theta^*_{\Lambda\pi}$ plot of Figs. 5, *a* and *b* shows a strong enhancement in the Y_1^* region at large $\cos\theta^*_{\Lambda\pi}$ values, together with an essentially complete forward-backward asymmetry in the repartition of the $\bar{\Lambda}\pi$ and $\Lambda\pi$ momentum vectors,

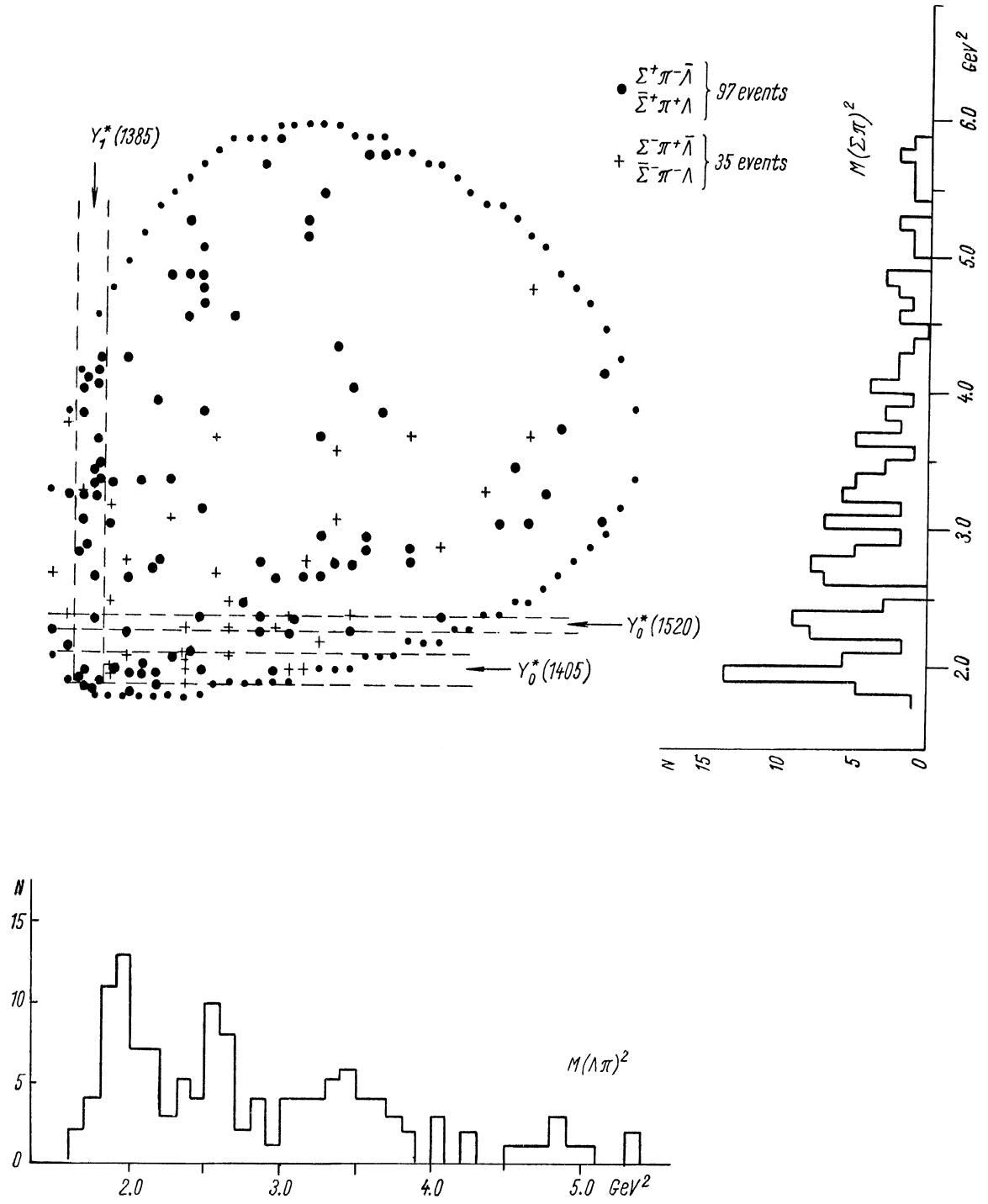

Fig. 3. Dalitz plot for $\Sigma\bar{\Lambda}\pi$, $\bar{\Sigma}\Lambda\pi$ final states.

respectively. Moreover, the excess of Y_1^{*+} ($\overline{Y_1^{*+}}$) over the Y_1^{*-} ($\overline{Y_1^{*-}}$), apparent in the mass plot of Figs. 5, *a* and *b*, can be entirely accounted for be an excess of associated production of Y_1^{*+} $\overline{Y_1^{*+}}$ pairs. Evidence for associated $Y_1^* \overline{Y_1^*}$ production is contained in Figs. 6, *a* and *b*, where the population of points in the crossing Y_1^*, $\overline{Y}_1^*$ bands is enhanced with respect to that expected from the background contribution. In more detail, there are 25 events of the type $Y_1^{*+}\overline{Y_1^{*+}}$ versus $12 Y_1^{*-}\overline{Y_1^{*-}}$ while the background is unlikely to exceed 6 of each type. This yields a ratio $Y_1^{*+}\overline{Y_1^{*+}}/Y_1^{*-}\overline{Y_1^{*-}}$ of 19/6.

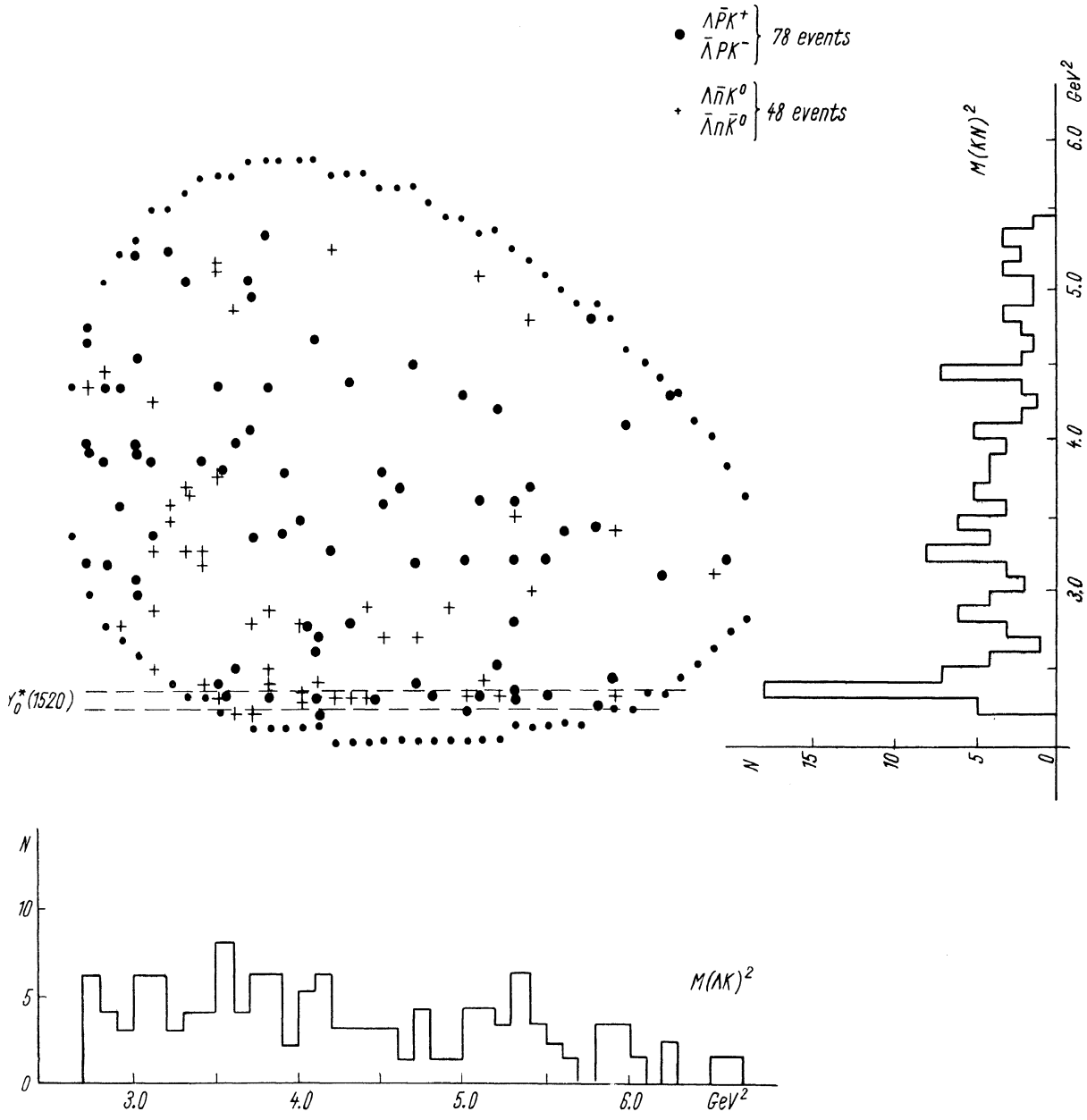

Fig. 4. Dalitz plot for $\Lambda\bar{N}K$, $\bar{\Lambda}N\bar{K}$ final states.

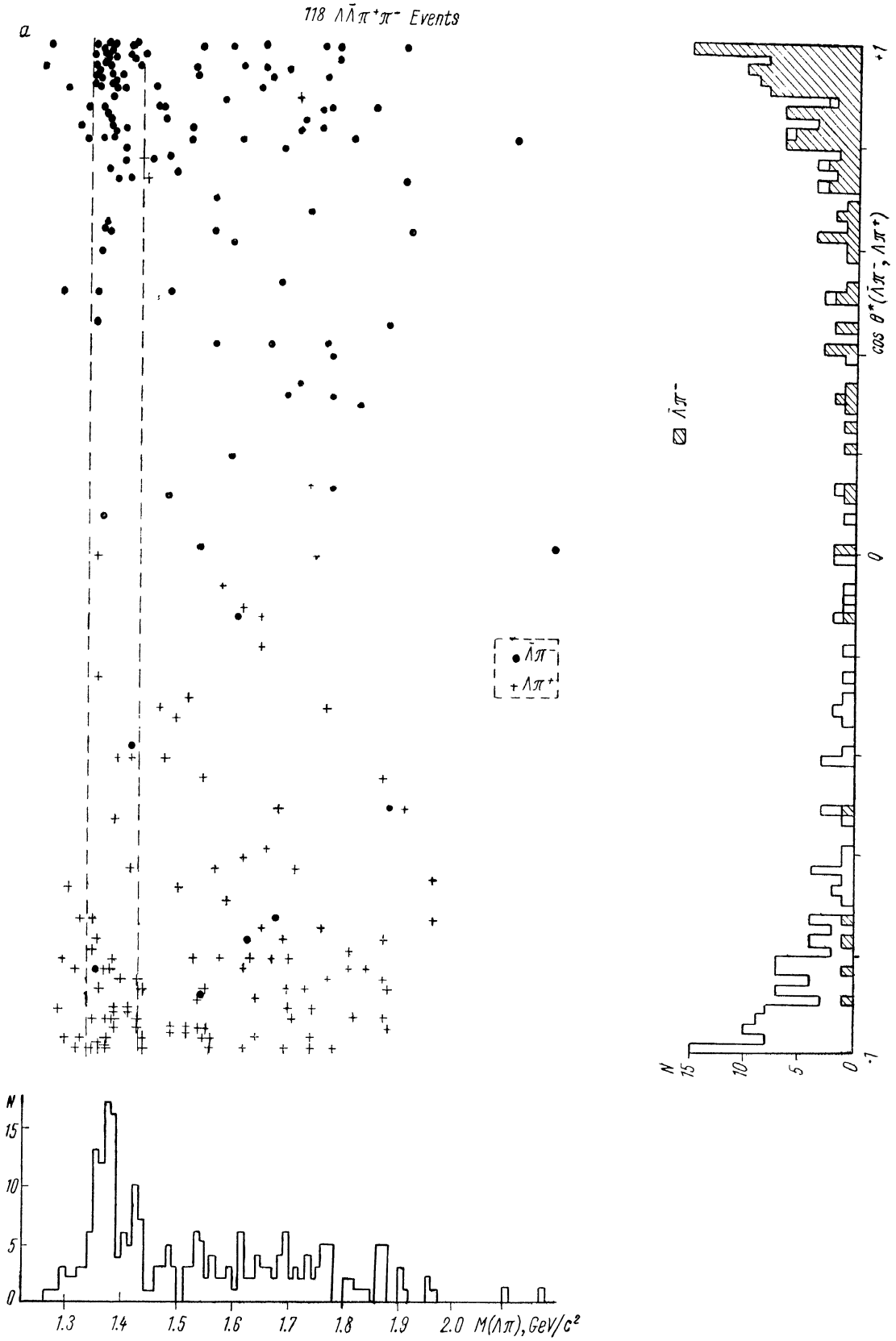

Fig. 5. Scatter plot of the invariant $\Lambda\pi$, $(\bar{\Lambda}\pi)$ mass versus $\cos\theta^*_{\Lambda\pi}$ for $\Lambda\bar{\Lambda}\pi^+\pi^-$ events.

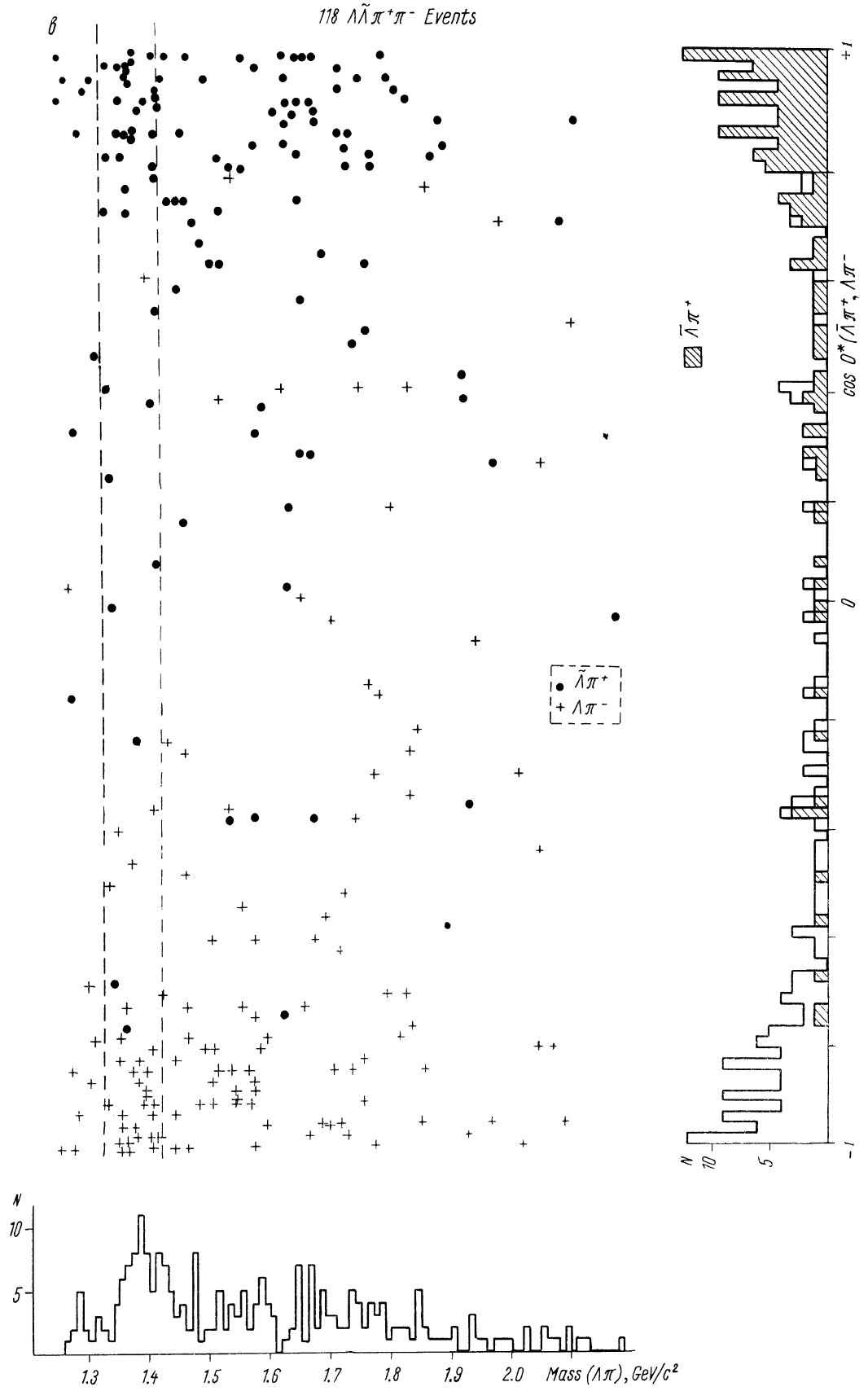

Fig. 5 (continued).

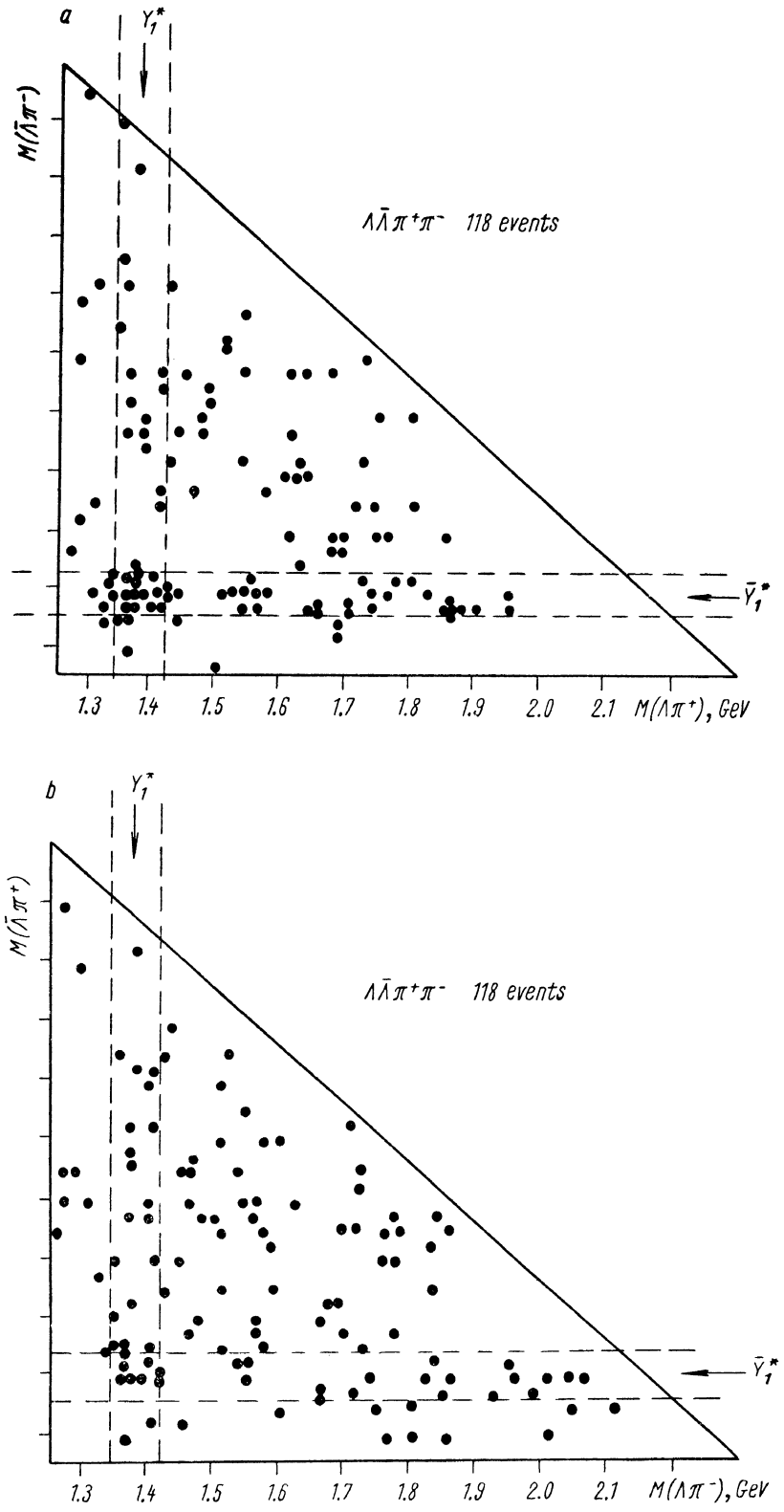

Fig. 6. Correlation plot between the $\Lambda\pi^+(\bar{\Lambda}\pi^-)$ and $\bar{\Lambda}\pi^+(\Lambda\pi^-)$ invariant-mass combinations for $\Lambda\bar{\Lambda}\pi^+\pi^-$ events.